Model-Based Robotic Cell Aspiration: Tackling Nonlinear Dynamics and Varying Cell Sizes

Guanqiao Shan , Zhuoran Zhang , Changsheng Dai , Xian Wang , Lap-Tak Chu, and Yu Sun

Abstract—Aspirating a single cell from the outside to the inside of a micropipette is widely used for cell transfer and manipulation. Due to the small volume of a single cell (picoliter) and nonlinear dynamics involved in the aspiration process, it is challenging to accurately and quickly position a cell to the target position inside a micropipette. This letter reports the first mathematical model that describes the nonlinear dynamics of cell motion inside a micropipette, which takes into account oil compressibility and connecting tube's deformation. Based on the model, an adaptive controller was designed to effectively compensate for the cell position error by estimating the time-varying cell medium length and speed in real time. In experiments, small-sized cells (human sperm, head width: ∼3 μm), medium-sized cells (T24 cancer cells, diameter: ∼15 μm), and large-sized cells (mouse embryos, diameter: ∼90 μm) were aspirated using different-sized micropipettes for evaluating the performance of the model and the controller. Based on aspirating 150 cells, the model-based adaptive control method was able to complete the positioning of a cell inside a micropipette within 6 seconds with a positioning accuracy of ±3 pixels and a success rate higher than 94%.

Index Terms—Biological Cell Manipulation, Automation at Micro-Nano Scales.

I. INTRODUCTION

CELL aspiration is a widely used technique for cell manipulation. It enables the transfer of a cell from one location to another for gene sequencing or protein measurement [1]. In clinical vitrification, an embryo is picked up by a micropipette and placed in different cryoprotectants for cryopreservation [2]. In animal cloning and IVF treatment, a somatic cell [3] or a single sperm [4] is aspirated into a micropipette and then deposited into an oocyte.

To perform the task of cell aspiration, a micropipette approaches a target cell, and by changing the piston position of an oil pump, the pressure applied to the micropipette tip is controlled to aspirate the cell into the micropipette. The cell
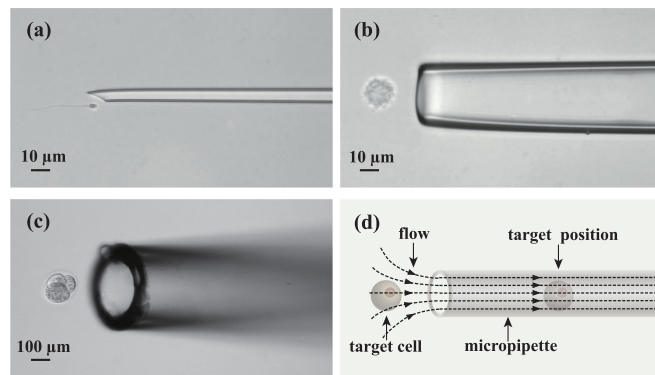
Fig. 1. Micropipette aspiration of different-sized cells. (a) A micropipette with the diameter of 5 μm is used to aspirate a human sperm. (b) A 25 μm micropipette is used to aspirate a T24 cancer cell. (c) A 125 μm micropipette is used to aspirate a mouse embryo. (d) A cell enters a micropipette driven by the surrounding medium flow which is controlled by changing the piston position of an oil pump.

is then moved to the target position inside the micropipette. In biology labs and clinics, the diameter of the micropipette tip ranges from 5 μm to over 100 μm for aspirating cells of different sizes (see Fig. 1). Due to the small volume of a cell, the travelling of the cell from the micropipette orifice to the target position inside the micropipette occurs within sub-seconds. Thus, in manual operation, a cell typically enters far into the micropipette and often disappears.

Robotic systems have been developed to perform cell aspiration [5]–[16]. In these systems, oil was treated as incompressible and the connecting tube between pump and micropipette was treated as rigid. Thus, the controllers were designed under the assumption that the cell medium volume change inside the micropipette was equal to the oil volume change caused by the piston movement of the oil pump. However, this assumption is flawed. In fluid mechanics, it is known when using an oil pump to regulate the flow inside a micrometer-sized channel, the flow rate inside the microchannel is lower than that produced by the pump [17]. This phenomenon is caused by the compressibility of oil and the elastic deformation of the connecting tube at the micro scale [18]–[20]. The negligence of oil compressibility and connecting tube's deformation can lead to significant inaccuracies in predicting the actual flow rate in the micropipette from the pump's piston movement. Therefore, previous robotic cell aspiration systems exhibited large overshoot (e.g., 200% overshoot vs. target position in [7]) and low success rate (e.g., 80.24% in [5]).

To significantly improve robotic cell aspiration, cell dynamics inside the micropipette needs to be better understood. In practice, the initial cell medium length is different every time before aspiration, and the cell medium length and speed also changes during aspiration. According to the Hagen-Poiseuille law [21], changes of the cell medium length and speed inside the micropipette lead to changes in pressure required to move the cell medium. The viscous effect of the Newtonian fluid (cell medium) causes substantial pressure variations and correspondingly, strong density changes inside the micropipette. Thus, the assumption that the cell medium volume change inside the micropipette is equal to the oil volume change caused by the piston movement of the oil pump does not hold.

This letter presents a nonlinear cell dynamics model, based on which an adaptive controller was designed to accurately control the cell position inside a micropipette. The controller effectively compensates for the positioning error by estimating cell medium length and speed in real time. We also confirmed that the dynamics model and control method have general applicability to the aspiration and positioning of cells of different sizes. Human sperm (small-sized cells), T24 cancer cells (medium-sized cells) and mouse embryos (large-sized cells) were robotically aspirated using different-sized micropipettes for evaluating the accuracy of the model and the performance of the controller. Based on aspirating 150 cells, the model-based adaptive control method was able to complete the positioning of a cell inside a micropipette within 6 seconds with a positioning accuracy of ± 3 pixels and a success rate higher than 94%.

II. DYNAMICS OF CELL MOTION

The dynamics of cell motion inside a micropipette is currently poorly understood. When the speed of flow is <30% of the speed of sound, the flow is typically treated as incompressible [17]. Under this assumption, it seems that the cell medium volume change inside the micropipette tip should be equal to the oil volume change caused by the piston movement of the oil pump. However, when the viscous liquid (i.e., cell medium) flows from a large channel (e.g., a petri dish) into a micropipette tip having a cross-section at the micrometer scale, pressure changes abruptly due to the viscous effect although the fluid speed is far less than 30% Mach number [17], [18]. Corresponding to the pressure change is a strong density change, resulting in oil compression and elastic deformation of the connecting tube. Therefore, when aspirating a cell using a micropipette, the cell medium volume change inside the micropipette tip is not equal to the oil volume change caused by the piston movement of the oil pump.

The dynamics model of cell motion developed here takes into account the compressibility of oil and the elastic deformation of the connecting tube. Fig. 2 shows the schematic of a general cell aspiration setup. It consists of an oil pump, a connecting tube, and a micropipette. The cell moves together with the cell medium (no relative motion), and its position is controlled by the piston movement of the oil pump. During cell aspiration and dispensing, the volume of the cell medium inside the micropipette changes as
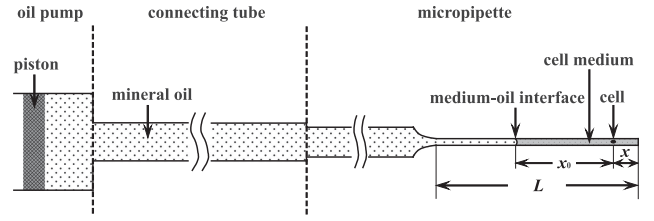
$$\Delta V = \Delta V_P - \Delta V_E \tag{1}$$

Fig. 2. Schematic of a general cell aspiration setup.

where ΔV_P is the volume change inside the pump, controlled by the piston movement; and ΔV_E is the volume change caused by the oil compressibility and elastic deformation of the connecting tube. The volume change ΔV_{E1} caused by oil compressibility is [18]

$$\Delta V_{E1} = -\frac{V}{E_V}\Delta p \tag{2}$$

where V is the volume of the oil in the whole system, E_V is the bulk modulus of the oil, and Δp is the pressure change applied to the oil. The oil volume inside the micropipette tip is neglected. Thus, Δp is equal to the pressure change applied to the end of the tip. The oil volume change ΔV_{E2} caused by connecting tube's deformation is [22]

$$\Delta V_{E2} = \frac{\pi l d^3}{4hE}\Delta p \tag{3}$$

where l and d are the length and inner diameter of the connecting tube, respectively; h is the thickness of the connecting tube's wall, and E is the Young's modulus of the tube's material (e.g., polyethylene). According to the Hagen-Poiseuille equation [21], when the viscous cell medium moves inside the micropipette tip at the speed of v, the pressure p applied to the end of the tip is

$$p = \frac{8\pi v \left[\mu_m L_m + \mu_o \left(L - L_m\right)\right]}{S} + p_0 \tag{4}$$

where μ_m and μ_o are the viscosity of the cell medium (i.e., 0.024 Pa·s) and mineral oil (i.e., 0.007 Pa·s), respectively; L_m is the cell medium length inside the micropipette tip, and L and S are the length and cross-sectional area of the micropipette tip, respectively; and p_0 is the constant pressure at the micropipette orifice.

In (4), the first term is the pressure loss which is proportional to the cell medium length and speed. This pressure loss acts as damping to suppress cell medium movement inside the micropipette. Substituting (2)–(4) into (1) and dividing the resultant equation by Δt result in

$$\begin{aligned} \frac{8\pi}{S}\left(\frac{V}{E_V} + \frac{\pi l d^3}{4hE}\right) &\left[\mu_m\left(L_m a + v^2\right)\right. \\ &\left. + \mu_o\left(La - L_m a - v^2\right)\right] + Sv = \alpha u \end{aligned} \tag{5}$$

where α is a coefficient to be calibrated experimentally. It describes the oil volume aspirated or dispensed by the oil pump per rotational degree of the knob. u is the input angular velocity of the pump's knob. v and a are the velocity and acceleration of the cell moving inside the micropipette.

To aspirate single cells of different sizes, the cross-sectional area of the micropipette S is a key factor to determine the dynamics of cell motion inside a micropipette. When S is small, the first term on the left-hand side in (5) is dominant over the second term, and the dynamics of cell motion exhibits nonlinearity caused by the change of the cell medium length and speed. As S increases (i.e., a large micropipette tip), the second term becomes more dominant over the first term, and thus the system linearity increases. This explains why using an oil pump to control the flow inside a microchannel (e.g., a micropipette tip), the flow rate inside the microchannel is lower than that produced by the oil pump; however, when the microchannel size is increased, for instance, to the millimeter scale, the flow rate inside the channel becomes identical to that produced by the oil pump.

III. CONTROLLER DESIGN

The task is to aspirate a cell into the micropipette and accurately position it at the target position within a short time. During aspiration, the cell medium length L_m changes with time, and the cell medium speed (i.e., cell speed) v also changes with time because it has a starting value when entering micropipette tip and eventually becomes zero when the cell reaches the target position. The changes of the cell medium length and speed cause system damping to change and thus affect the cell positioning performance. To address this problem, a robust controller assumes that the uncertainty of the system is bounded. Since in a cell aspiration system, it is difficult to estimate the range of the cell medium length and speed, relatively large ranges need to be set to guarantee the positioning error to be asymptotic to zero, which would sacrifice the settling time (to be quantitatively discussed in the Results section).

Thus, considering time-varying cell medium length and speed, a model-based adaptive control is designed in this work. The adaptive controller estimates and updates the cell medium length and speed in real time, and compensates for the position error based on the dynamics model of cell motion. To design the adaptive control law, the dynamics of cell motion described in (5) is rewritten as

$$\beta \left[(\mu_m - \mu_o) L_m + \mu_o L\right] \ddot{x}$$
$$+ \left[\beta (\mu_m - \mu_o) \dot{x} + \frac{S}{\alpha}\right] \dot{x} = u \tag{6}$$

where

$$\beta = \frac{8\pi}{\alpha S} \left(\frac{V}{E_V} + \frac{\pi l d^3}{4hE}\right)$$

x is the cell's position inside the micropipette tip. Cell medium length $L_m = x + x_0$, where x_0 is the initial cell medium length before cell entrance into the micropipette tip.

In (6), there are three types of parameters. The first type is all set constant when the aspiration system is set up, such as β, μ_0 and μ_m, L, S, and α. The second type is constant for each aspiration operation, but different between two aspiration operations, such as the initial cell medium length x_0. In practice, x_0 is different every time before aspiration starts, it can be different by >100 μm; therefore, using a constant value for x_0

for every aspiration operation degrades the control performance. Hence, x_0 must be determined for each aspiration operation individually. The third type includes parameters that dynamically change during aspiration, such as x and $\dot{x}$. These parameters are the factors that cause nonlinearity of the aspiration system. Thus, (6) is rewritten into a linear part and a nonlinear part.

$$\left(\bar{\theta}_1 + \tilde{\theta}_1\right) \ddot{x} + \left(\bar{\theta}_2 + \tilde{\theta}_2\right) \dot{x} = u \tag{7}$$

where $\bar{\theta}_1 = \beta[(\mu_m - \mu_o)x_0 + \mu_o L]$, $\bar{\theta}_2 = \beta(\mu_m - \mu_o)\dot{x}_0 + S/\alpha$, $\tilde{\theta}_1 = \beta(\mu_m - \mu_o)x$, and $\tilde{\theta}_2 = \beta(\mu_m - \mu_o)(\dot{x} - \dot{x}_0)$. $\bar{\theta}_1$ and $\bar{\theta}_2$ are constant, and $\tilde{\theta}_1$ and $\tilde{\theta}_2$ are functions of x and $\dot{x}$, respectively, both of which dynamically change during the cell aspiration process. $\dot{x}_0$ is the initial speed of the cell at the time instance when it enters the micropipette tip.

The adaptive control law u consists of a feedback term u_1 and a model compensation term u_2

$$u = u_1 + u_2, \tag{8}$$

$$u_1 = k_p e + k_d \dot{e} \tag{9}$$

and

$$u_2 = \frac{\tilde{\theta}_1}{\bar{\theta}_1} \left(k_p e + k_d \dot{e} - \bar{\theta}_2 \dot{x}\right) + \tilde{\theta}_2 \dot{x} \tag{10}$$

where $e = x_d - x$ is the position error, x_d is the target position, and k_p and k_d are feedback gains. Compensation term u_2 updates $\tilde{\theta}_1$ and $\tilde{\theta}_2$ by $\beta(\mu_m - \mu_o)x$ and $\beta(\mu_m - \mu_o)(\dot{x} - \dot{x}_0)$ in real time, and compensates for the position error caused by system nonlinearity. Substituting (8)–(10) into (7) results in

$$\left(\bar{\theta}_1 + \tilde{\theta}_1\right) \ddot{x} + \left(\bar{\theta}_1 + \tilde{\theta}_1\right) \dot{x} = \left(\frac{\tilde{\theta}_1}{\bar{\theta}_1} + 1\right) (k_p e + k_d \dot{e})$$
$$+ \left(\tilde{\theta}_2 - \frac{\tilde{\theta}_1 \bar{\theta}_2}{\bar{\theta}_1}\right) \dot{x} \tag{11}$$

To find the control law of u for (11) is equivalent to finding the minimum of the linear-quadratic cost function

$$J = \int_{t_0}^{t_f} \left(X^T Q X + u_1^T R u_1\right) dt \tag{12}$$

for

$$\bar{\theta}_1 \ddot{x} + \bar{\theta}_2 \dot{x} = u_1 \tag{13}$$

where t_0 and t_f are the initial time and terminal time, respectively; Q and R are the relative weights on state and control; and $X = [x, \dot{x}]^T$. In (12), $X^T Q X$ represents the error of aspiration in terms of the target position; $u_1^T R u_1$ represents input energy for cell aspiration, which indicates the output power limitation of the pump motor.

Solving $\min\{J\}$ is then translated to a linear quadratic regulator (LQR) problem. Based on the LQR theory [23], the control law u_1 is

$$u_1^* = -KX = -R^{-1}B^T P X \tag{14}$$

where $K = [k_p, k_d]$ is the feedback parameter matrix, $B = [0, 1/\bar{\theta}_1]^T$ is the input coefficient matrix, and P is solved from
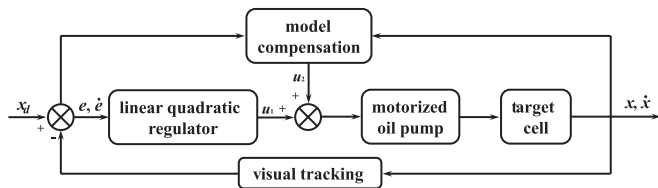
Fig. 3. Diagram of the model-based adaptive control system.

the Riccati equation

$$PA + A^T P + QPBR^{-1}B^T P + \dot{P} = 0 \qquad (15)$$

Substituting k_p and k_d into (9) and (10), the control law u is obtained.

In (8), the initial cell medium length x_0 and the initial speed of the cell $\dot{x}_0$ need to be calculated to start the adaptive controller. According to $(x_c - x_l)/t_0$, $\dot{x}_0$ is determined, where x_c is the position of the cell when it reaches the micropipette orifice, x_l is the last position of the cell before it reaches the micropipette orifice, and t_0 is the time interval between two image frames. The initial length of the cell medium x_0, in comparison, is difficult to determine from visual feedback because the field of view under a microscope is small and the cell medium-oil interface is usually out of the field of view when the cell reaches the micropipette orifice. To determine x_0, we command the oil pump to continue aspirating at a constant speed when the cell is outside the micropipette tip. At the moment when the cell enters the micropipette tip, x_0 is calculated according to (5).

The control diagram is shown in Fig. 3 with visual tracking providing feedback for the adaptive control system. To enhance the reliability of visual tracking when the cell is in the extreme proximity of micropipette orifice/edge, a reference frame is recorded before cell aspiration and used to subtract the micropipette edge information from each subsequent frame during cell aspiration. Visual tracking of a target cell can also be interfered by the movement of other motile cells (in the case of aspirating human sperm) or surrounding contaminants/particles. To address this issue, an adapted probabilistic data association filter algorithm [24] is used to reliably track the target cell.

IV. EXPERIMENTAL RESULTS AND DISCUSSION

Single cell aspiration experiments were performed on an inverted microscope (Nikon Eclipse Ti-S) with a micromanipulator (MX7600, Siskiyou) mounted on it. The micropipette was connected to an oil pump (CellTram Vario, Eppendorf Canada Ltd.) which was controlled by a stepper motor. The output of the oil pump was calibrated to be 2.3 nL per rotational degree. The total oil volume of the pump system was 1.5 mL. The inner diameter, outer diameter and length of the connecting polyethylene tube were 1 mm, 2.5 mm, and 1 m, respectively. A camera (scA1300-32gm, Basler) was connected to the microscope to obtain visual feedback. Images are captured in brightfield at 30 frames per second. Cell medium and cells were in a Petri dish into which the micropipette was immersed.

A. Model Validation

To evaluate the performance of the dynamics model of cell motion inside a micropipette, cell medium was aspirated into different-sized micropipettes. The flow rate produced by the motorized oil pump was 1 nL/s, and the initial cell medium length inside the micropipettes before aspiration was set to be 50 μm. The volume aspirated into the micropipette was calculated by $S\Delta x$. Δx is the position change of the medium-oil interface, for which the orifice of the micropipette was intentionally moved out of the microscope's field of view to observe the medium-oil interface. Fig. 4 summarizes the model-predicted cell medium volume aspirated into the micropipette vs. experimentally measured cell medium volume. For the three different-sized micropipettes, the root-mean-square errors (RMSEs) were 0.0012 pL, 1.0615 pL, and 8.1 pL, respectively.

As shown in Fig. 4(a)(b), for small micropipettes (5 μm and 25 μm), nonlinearity of cell medium volume vs. time is apparent. At the end of 1 s aspiration, the volume change produced by the oil pump was 1 nL while the volume change inside the micropipette was 0.17 pL (for 5 μm micropipette) and 99.6 pL (for 25 μm micropipette), with both being significantly lower than 1 nL. According to (5), when S is small, the first term on the left-hand side dominates, and the volume discrepancy was caused by oil compressibility and elastic deformation of the connecting tube. As S increases, the second term in (5) becomes more dominant. The influence of oil compressibility and tube deformation becomes less. Since the second term is linear, the dynamics of fluid motion is more linear and independent of the change of the cell medium length and speed. As shown in Fig. 4(c), the flow rate inside the 125 μm micropipette was a constant value (0.998 nL/s) and was almost identical to the flow rate of 1 nL/s produced by the motorized oil pump.

We also experimentally varied the initial length of the cell medium x_0 to investigate its effect on the dynamics of fluid motion inside the micropipette. In these experiments, the flow rate produced by the motorized oil pump was fixed at 1 nL/s for the micropipettes of different sizes, and x_0 was varied from 50 μm to 150 μm for each micropipette size. For a 5 μm micropipette, as x_0 increased from 50 μm to 150 μm, for each time instance, the flow rate inside the micropipette (quantified by measuring the medium-oil interface position change over time) became lower. At the end of 1 s aspiration, the displacement of the medium-oil interface was 10.7 μm for $x_0 = 50$ μm but was only 8.3 μm for $x_0 = 150$ μm. Therefore, in order to displace a cell for an equal distance within the same time duration, the oil pump needs to produce a higher flow rate for a larger x_0. In contrast, for a 125 μm micropipette, the medium-oil interface position change was independent of the initial cell medium length x_0, and the system became a first-order time-invariant linear system.

B. Control Performance

To quantify the performance of model-based robotic cell aspiration, human sperm, T24 cells and mouse embryos were aspirated by 5 μm, 25 μm and 125 μm micropipettes under the microscope objective of 40X (1 pixel = 0.21 μm), 20X (1 pixel = 0.42 μm) and 4X (1 pixel = 2.1 μm), respectively.
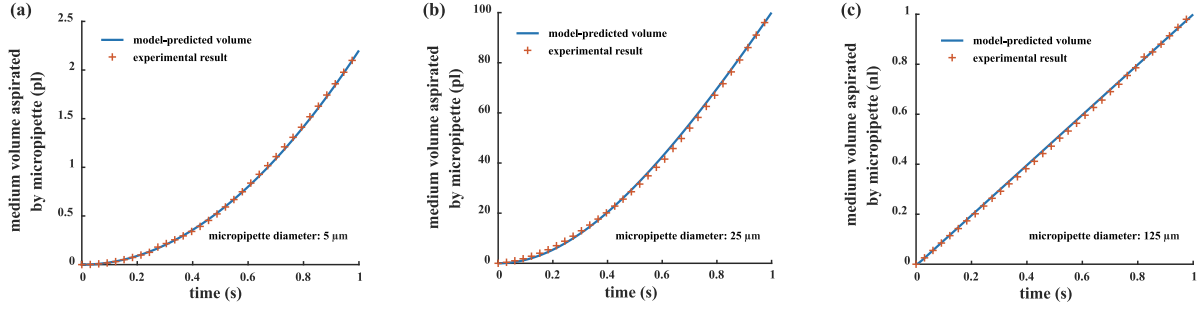
Fig. 4. Model-predicted cell medium volume aspirated into micropipette vs. experimental measurements, for micropipettes with different diameters: (a) 5 μm, (b) 25 μm, and (c) 125 μm. In these experiments, the flow rate produced by the oil pump was 1 nL/s. The initial medium length x_0 inside the micropipette before aspiration was 50 μm.
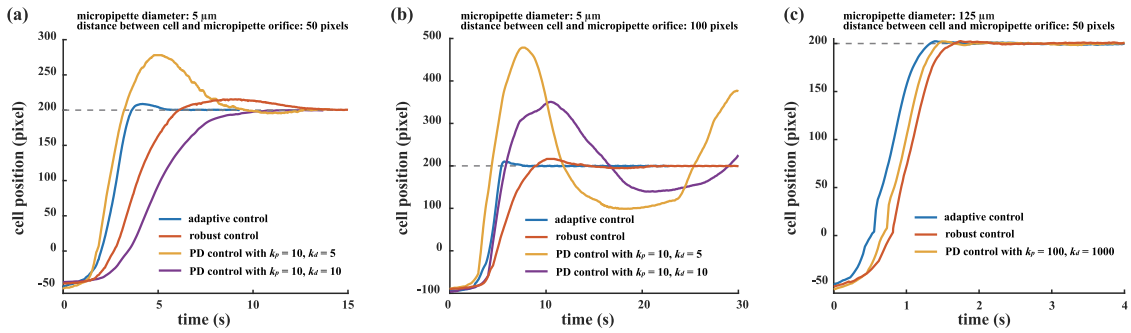

Fig. 5. Control performance of adaptive control, robust control, and PD control. (a) Micropipette diameter: 5 μm; and distance between target cell and micropipette orifice: 50 pixels. (b) Micropipette diameter: 5 μm; and distance between target cell and micropipette orifice: 100 pixels. (c) Micropipette diameter: 125 μm; and distance between target cell and micropipette orifice: 50 pixels. The oil pump aspirated the cell at the flow rate of 5 nL/s until the cell reached the micropipette orifice.

The orifice of the micropipette tip was defined as the origin, and the target position was set to be 200 pixels from the origin. When the target cell was outside the micropipette, the motorized oil pump performed aspiration at a constant flow rate. At the time instance when the cell reached the orifice, the initial cell medium speed was measured, and the initial cell medium length was calculated according to (5). The parameters k_p and k_d of the adaptive controller were then determined, and the controller started to operate.

Four metrics were used to quantify the system's performance, including success rate, positioning accuracy, overshoot, and settling time. Success rate was defined by the number of cells that did not travel outside the microscope's field of view over the total number of cells that were aspirated. Positioning accuracy was the steady-state positioning error relative to the target position. Settling time was the entire time period required for aspirating a cell into the micropipette and positioning it at the target position. Overshoot was defined by the farthest cell position exceeding the target position in the micropipette.

In experiments, 50 cells for each of the three cell types were aspirated with their corresponding-sized micropipette. The success rates were 94%, 96%, and 100% for the aspiration of human sperm, T24 cells, and mouse embryos by the adaptive controller. Failure occurred for a few of the cells that adhered more strongly on the substrate than the majority of the cells. In those cases, the oil pump performed aspiration at a constant flow rate for an overly long time period. When the cell reached

the orifice of the micropipette tip, its velocity was too high, leaving the controller no time to decelerate the cell, and the cell went far into the micropipette and disappeared from the field of view. The cell positioning accuracy was quantified to be ±3 pixels, i.e., ±0.625 μm, ±1.25 μm and ±6.25 μm under 40X (for human sperm aspiration), 20X (for T24 cell aspiration), and 4X (for mouse embryo aspiration), respectively. The average settling time was 6 s, 6 s and 2 s. The largest overshoot was 9 pixels, 10 pixels, and 3 pixels.

The model-based adaptive control was also compared with PD control and robust control. The PD control gains were optimized based on extensive empirical tuning. For robust control, the control law was designed according to (7). The uncertainty ranges of $\tilde{\theta}_1$ and $\tilde{\theta}_2$ were defined by $[0, \beta(\mu_m - \mu_o)x_d]$ and $[-\beta(\mu_m - \mu_o)\dot{x}_0, 0.5\beta(\mu_m - \mu_o)\dot{x}_0]$. Fig. 5(a) shows the aspiration of a single human sperm with a 5 μm micropipette, where one can see that the PD controller required a longer settling time than the adaptive controller (12 s vs. 6 s) when a large derivative gain (e.g., $k_d = 10$) was used. As the derivative gain was reduced ($k_d = 5$), the overshoot of the PD controller increased dramatically (from 9 pixels to 78 pixels). The overshoot of the robust controller was small (16 pixels), but it required a longer settling time (14 s vs. 6 s). Compared to PD control and robust control, the model-based adaptive control achieved smaller overshoot and shorter settling time.

During cell aspiration, a cell first accelerated when entering the micropipette, then decelerated when approaching the target

position, and stopped at the target position at last. Because the cell medium length and speed changed with time, system damping was time-varying. According to (4), the damping first increased during the cell's acceleration period and early deceleration period, and then decreased to zero during the rest of cell's deceleration period. The adaptive controller estimated the cell medium length and speed in real time. Based on the dynamics model of cell motion, the term u_2 estimated the current system damping and compensated for the control output. Therefore, the variation of system damping was well tackled by the adaptive controller. However, for a PD controller, system damping was treated as constant. When a low system damping was assumed and a large derivative gain was used, the cell's acceleration was small and the cell slowed down quickly while it was far away from the target position (see the purple curve in Fig. 5(a)). On the contrary, when a large system damping was assumed and a small derivative gain was used, the cell's deceleration was small and the cell was unable to stop at the target position within a short time, and thus produced a large overshoot (see the yellow curve in Fig. 5(a)). The robust controller took into account variations of cell medium length and speed; however, to guarantee the positioning error to be asymptotic to zero, its derivative gain was large so that the real part of each pole of the system was negative within the predefined uncertainty ranges. Therefore, similar to the PD controller with a large derivative gain, it required a long settling time.

To further compare the control performance of the three controllers, the distance between the target cell and the micropipette orifice was intentionally increased from 50 pixels to 100 pixels. Increasing the distance caused the increase of the initial cell medium length and speed when the cell reached the orifice. Thus, the variation range of cell medium length and speed changed. As shown in Fig. 5(b), the model-based adaptive controller maintained a small overshoot (9 pixels) and a short settling time ($\sim$6 s). The performance of the PD controller with the same control parameters as used in Fig. 5(a) degraded dramatically. The PD controller was unable to control the system with the damping change, and oscillation persisted for a long time period. The robust controller still maintained a small overshoot (16 pixels), but had a long settling time ($\sim$18 s).

For a large micropipette (diameter: 125 μm) to aspirate a large cell such as a mouse embryo, the three controllers showed comparable performance with a short settling time around 2 s, and a small overshoot less than 3 pixels, as shown in Fig. 5(c). According to Section IV-A, when using a large micropipette, the system became a first-order time-invariant linear system, and the dynamics of cell motion was independent of the variations of cell medium length and speed (see Fig. 4(c)). Therefore, the advantage of the model-based adaptive controller became less apparent than the robust controller and PD controller.

V. CONCLUSION

This letter presented a dynamics model describing cell motion aspirated from the outside to the inside of a micropipette. Based on this model, a model-based adaptive control method was developed for automated cell aspiration and positioning inside a micropipette. Experimental results revealed that the controller

effectively compensated for the cell positioning error by estimating cell medium length and speed in real time. The success rates were 94%, 96%, and 100% for the aspiration of human sperm, T24 cells, and mouse embryos with an accuracy of $\pm$3 pixels. Compared to PD controller and robust controller, the adaptive controller achieved smaller overshoot and shorter settling time. The achieved largest overshoot was 9 pixels, 10 pixels, and 3 pixels and the average settling time was 6 s, 6 s and 2 s for the aspiration of the three different types of cells.

REFERENCES

[1] S. Ishii, K. Tago, and K. Senoo, "Single-cell analysis and isolation for microbiology and biotechnology: Methods and applications," *Appl. Microbiology Biotechnology*, vol. 86, no. 5, pp. 1281–1292, 2010.

[2] Z. P. Nagy *et al.*, *Cryopreservation of Mammalian Gametes and Embryos: Methods and Protocols*. Berlin, Germany: Springer, 2017.

[3] Z. Liu *et al.*, "Cloning of macaque monkeys by somatic cell nuclear transfer," *Cell*, vol. 172, no. 4, pp. 881–887, 2018.

[4] P. Rubino *et al.*, "The ICSI procedure from past to future: A systematic review of the more controversial aspects," *Human Reproduction Update*, vol. 22, no. 2, pp. 194–227, 2015.

[5] Z. Lu *et al.*, "Single cell deposition and patterning with a robotic system," *PLoS One*, vol. 5, no. 10, 2010, Art. no. e13542.

[6] Z. Lu, X. Zhang, C. Leung, N. Esfandiari, R. F. Casper, and Y. Sun, "Robotic ICSI (intracytoplasmic sperm injection)," *IEEE Trans. Biomed. Eng.*, vol. 58, no. 7, pp. 2102–2108, Jul. 2011.

[7] X. P. Zhang, C. Leung, Z. Lu, N. Esfandiari, R. F. Casper, and Y. Sun, "Controlled aspiration and positioning of biological cells in a micropipette," *IEEE Trans. Biomed. Eng.*, vol. 59, no. 4, pp. 1032–1040, Apr. 2012.

[8] J. Liu *et al.*, "Automated vitrification of embryos: A robotics approach," *IEEE Robot. Autom. Mag.*, vol. 22, no. 2, pp. 33–40, Jun. 2015.

[9] I. Paranawithana, W. Yang, and U. Tan, "Tracking extraction of blastomere for embryo biopsy," in *Proc. IEEE Int. Conf. Robot. Biomimetics*. IEEE, 2015, pp. 380–384.

[10] Z. Zhang *et al.*, "Robotic pick-and-place of multiple embryos for vitrification," *IEEE Robot. Autom. Lett.*, vol. 2, no. 2, pp. 570–576, Apr. 2017.

[11] J. Zhu, L. Gao, P. Pan, Y. Wang, R. Chen, and C. Ru, "Study of robotic system for automated oocyte manipulation," in *Proc. Int. Conf. Manipulation, Autom. Robot. Small Scales*. IEEE, 2017, pp. 1–6.

[12] C. Y. Wong and J. K. Mills, "Cell extraction automation in single cell surgery using the displacement method," *Biomed. Microdevices*, vol. 21, no. 3, p. 52, 2019.

[13] Y. Kasai, S. Sakuma, and F. Arai, "Isolation of single motile cells using a high-speed picoliter pipette," *Microfluidics Nanofluidics*, vol. 23, no. 2, p. 18, 2019.

[14] H. Wang *et al.*, "Three-dimensional autofocusing visual feedback for automated rare cells sorting in fluorescence microscopy," *Micromachines*, vol. 10, no. 9, p. 567, 2019.

[15] Z. Nan, Q. Xu, Y. Zhang, and W. Ge, "Force-sensing robotic microinjection system for automated multi-cell injection with consistent quality," *IEEE Access*, vol. 7, pp. 55543–55553, 2019.

[16] Z. Zhang, X. Wang, J. Liu, C. Dai, and Y. Sun, "Robotic micromanipulation: Fundamentals and applications," *Annu. Rev. Control, Robot., Auton. Syst.*, vol. 2, pp. 181–203, 2019.

[17] M. Gad-el Hak, "The fluid mechanics of microdevices," *J. Fluids Eng.*, vol. 121, no. 1, pp. 5–33, 1999.

[18] P. Tabeling, *Introduction to Microfluidics*. Oxford, U.K.: OUP, 2005.

[19] H. A. Stone, A. D. Stroock, and A. Ajdari, "Engineering flows in small devices: Microfluidics toward a lab-on-a-chip," *Annu. Rev. Fluid Mech.*, vol. 36, pp. 381–411, 2004.

[20] P. Burriel *et al.*, "Bottleneck effect in two-dimensional microfluidics," *Physical Rev. Lett.*, vol. 100, no. 13, 2008, Art. no. 134503.

[21] R. A. Chilton and R. Stainsby, "Pressure loss equations for laminar and turbulent non-Newtonian pipe flow," *J. Hydraulic Eng.*, vol. 124, no. 5, pp. 522–529, 1998.

[22] V. S. Á. Salazar, A. Medina, and J. Klapp, "Deformation profiles of elastic cylindrical tubes filled with granular media under an overload," in *Proc. EPJ Web Conf. EDP Sciences*, vol. 140, 2017, Art. no. 02025.

[23] F. Lin, *Robust Control Design: An Optimal Control Method*. New York, NY, USA: Wiley, 2007.

[24] Z. Zhang *et al.*, "Robotic immobilization of motile sperm for clinical intracytoplasmic sperm injection," *IEEE Trans. Biomed. Eng.*, vol. 66, no. 2, pp. 444–452, Feb. 2019.